ISSN 2176-5480

22nd International Congress of Mechanical Engineering (COBEM 2013)
November 3-7, 2013, Ribeirão Preto, SP, Brazil

DESCRIPTION OF THE SHAPE OF LONG BUBBES IN HORIZONTAL TURBULENT SLUG FLOW

L.M.C. Matamoros
J.B.R. Loureiro
A.P. Silva Freire
Mechanical Engineering Program (COPPE/UFRJ), C.P. 68503, 21945-970, Rio de Janeiro, Brazil

Abstract. *The shapes of long bubbles in horizontal turbulent slug flows is experimentally investigated through the shadow sizing technique. The flow conditions were set to produce very long and interface perturbed bubbles. A special procedure was developed to correctly identify the lengths, areas and volumes of the bubbles. The procedure is capable of furnishing a complete characterization of the three-dimensional aspects of the bubble, including its interface area. Image treatment and calculation procedures were developed within the framework of the Wolfram's Mathematica 8.0 software package. The experimental results are compared with the theory of Netto et al. (1999). For the first time, characteristic volumes and areas of long bubbles in slug flows are correlated through simple power-law expressions.*

Keywords: *Horizontal Slug Flow, Interfaces, Experimental methods, Optical Techniques.*

1. INTRODUCTION

Slug flows are the predominant flow pattern in the petroleum industry. Hence, their physical and mathematical modelling is of utmost importance for the design and operation of equipment and facilities.

Despite the inherent complexities in the structure of slug flows, some authors have proposed one-dimensional models based on mechanistic arguments to describe the flow dynamics. The models are usually formulated in terms of sixteen flow variables, four physical properties and two geometric parameters that characterize pipe size and orientation.

Unfortunately, one-dimensional models do not furnish the shape and volume of bubbles. This is a serious problem for applications that require knowledge of the interface area (Magalhaes et al. (2013)). To characterize the shape and volume of bubbles, a detailed theory is that of Netto et al. (1999).

In the present study, images captured at high frequencies are processed to obtain the shape, velocity, volume, dry area, wet area, interface area and length of the bubbles in horizontal slug flows. The results are compared to the model of Netto et al. (1999), which is here independently validated for the first time. The high resolution of the images shows the complexities of the interface between the gas and liquid phases, as a function of the Froude number based on the liquid velocity ahead of the bubble.

Because the theory of Netto et al. does not accounts for the interface fluctuations, the experimental interface area is always higher than the theoretical area; the present work shows this difference to be about 6%. Indeed, the theory of Netto et al. (1999) was developed for and tested against experiments that considered only isolate bubbles. The effects of flow turbulence on the shapes of noses and tails of long slug bubbles are also described.

To incorporate the interface effects onto one-dimensional theories, one possibility is to develop expressions of the form $l = f(V^{1/3})$ and $A = g(V^{2/3})$, where l stands for length, A for area and V for volume. Magalhaes et al. (2013) performed a very simplified experimental analysis to propose $A = 3.7V^{2/3}$ and $l = 271V^{2/3}$ - $2.4V^{1/3}$. The present very detailed study suggests otherwise that: $A/D^2 = 3.70(V^{2/3}/D^2)^{1.16}$ and $l/D = 3.12(V^{1/3}/D)^{2.48}$.

Concerning the experiments, images are defined through characteristic pixels with characteristic values that are used to define the contour of the bubbles. With the contour line of the bubbles, it is possible to define a mathematical transformation that determines the exact spatial location of each interface point and then evaluates volumes, areas and lengths. To perform the image processing, the computational platform WOLFRAM MATHEMATICA 8.0 is used.

2. THE THEORY OF NETTO ET AL.

The theory of Netto et al. (1999) is introduced next. Only the main aspects of the theory are considered.

In the following, bubble shapes are represented in terms of the liquid volume fraction (α_L) as a function of the distance to the bubble nose ($\xi = x/D$). Four distinct regions are identified: nose, main body, hydraulic jump and tail (Fig. 1). These regions must be patched at positions (ξ_i, α_{Li}), i = 0,1,2,3.

2.1 Nose

The nose solution is obtained through the inviscid theory of Benjamin (1968). With the condition $\xi < 1$, Benjamin's solution can be approximated by

ISSN 2176-5480

$$\alpha_L = 1 - 0.775\xi + 0.345\xi^2 \tag{1}$$

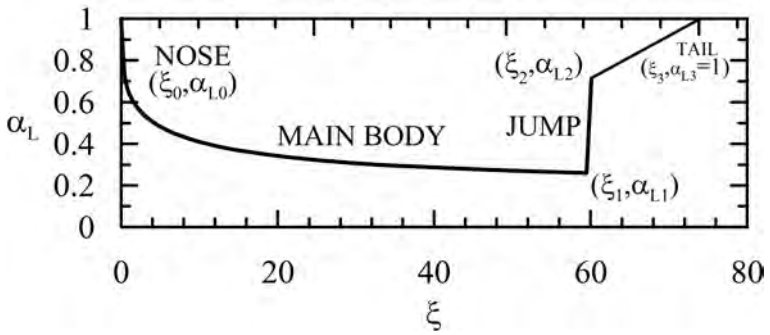

Figure 1. Bubble model according to Netto et al. (1999).

The general expression for the nose shape is much more complex than Eq. (1) (see the original reference or Netto et al. (1999)). However, for the present simulation, Eq. (1) is a good enough approximation.

2.2 Main body

The solution of the main body is based on the one-dimensional model of Andreussi et al. (1993). Mass and momentum conservation equations for each phase are solved under the assumption that the shape does not change with time and that far enough from the nose the liquid film is fully developed. The model resorts to closure laws for the wall and interface shear stresses and some simplifying hypotheses concerning long wave approximations to obtain,

$$\begin{aligned} &-(1+k/8)\ln\left(\frac{2\alpha_L+1}{2\alpha_{L0}+1}\right) + (1+k\alpha_{L\infty}^2(1.5+2\alpha_{L\infty}))\ln\left(\frac{\alpha_L-\alpha_{L\infty}}{\alpha_{L0}-\alpha_{L\infty}}\right) \\ &-\left(\frac{1-k\alpha_{L\infty}^3}{(\alpha_{L\infty}+0.5)(\alpha_{L0}-\alpha_{L\infty})(\alpha_L-\alpha_{L\infty})}-k\right)(\alpha_{L\infty}+0.5)^2(\alpha_L-\alpha_{L0}) = f_{L0}\left(\frac{\alpha_{L\infty}+0.5}{\alpha_{L\infty}}\right)^2(\xi-\xi_0) \end{aligned} \tag{2}$$

where

$$k = 0.82\frac{gD}{\varphi^2}, \quad \varphi = V - U\ (= \text{film velocity}) \tag{3}$$

$$\alpha_{L\infty} = 1.027(\varphi/V) + 0.054(\varphi/V)^2 \tag{4}$$

Quantity V denotes the nose velocity, U is the liquid velocity ahead of the bubble and the initial condition (ξ_0,α_{L0}) is obtained from the nose equation.

The body and nose solutions must be patched at a point where both solutions exhibit the same first derivative,

$$\begin{aligned} -\frac{d\alpha_L}{d\xi}|_{\alpha_{L0}} &= \frac{f_{L0}(\alpha_{L0}+0.5)}{1-k\alpha_{L0}^3}\left(\frac{\alpha_{L0}-\alpha_{L\infty}}{\alpha_{L\infty}}\right)^2 \\ &= 1.17(\alpha_{L0}-0.565)^{1/2} \end{aligned} \tag{5}$$

2.3 Hydraulic jump

The equation for the hydraulic jump is obtained from global balances of mass and momentum; it follows that

$$\frac{Fr_R^2}{\alpha_{L1}} + f(\alpha_{L1}) = \frac{Fr_R^2}{\alpha_{L2}} + f(\alpha_{L2}) - \frac{F_w}{\rho_L g D A} \tag{6}$$

where

ISSN 2176-5480

$$f(\alpha_L) = \int_0^{\alpha_L} d\alpha_L (H - z) D^{-1}, \tag{7}$$

Fr_R is the Froude number (= $\varphi/\sqrt{gD}$) and H the position of the interface.

For fixed values of Fr_R and α_{L1}, only one value of α_{L2} is furnished by Eq. (7). Provided $\alpha_{L2} \geq 1$, the hydraulic jump reaches the top wall so that no tail is formed (plug flow).

The force exerted by the wall on the liquid across the jump, F_W, depends of the flow pattern – whether slug or plug – and is obtained through experimental results ($F_w = C_J L_J S \tau_{L0}^W$, C_J = 4, L_J = D).

2.4 Tail

The shape of the tail depends on Fr. A simplified equation can be obtained considering at the extreme end, α_L = 1, and $d\alpha_L/dh$ = 0, so that

$$\frac{dh}{d\xi} = 2 f_{L0} \frac{U^2}{gD} = \text{ constant} \tag{8}$$

2.5 Model summary

The model of Netto et al. (1999) needs three inputs: pipe diameter, liquid flow velocity and bubble volume.

With the above equations, $\alpha_{L\infty}$ is initially found. Next, α_{L0} is determined. An iterative procedure is then used to find α_{L1} and α_{L2}.

3. EARLY WORK

Experimental analysis, of course, plays a fundamental role on the development of one-dimensional slug flow mechanistic predictive models. In addition to relations obtained from the first principles, further closure realtions must be obtained from empirical formulations.

The recent advances in digital electronics have introduced new equipment with particularly high spatial and temporal resolution. One of these devices is the high-speed digital camera. Depending on the model, up to 2000 thousand images per second can be captured. This feature has recently become very important to applications in scientific technological development, so much as one considers the recent advances in image treatment.

The analysis of multiphase flows greatly benefited in the past from classical high-speed filming, but the recent advances in image treatment have permitted new characteristics to be explored.

Many important flow variables, including velocity and typical frequency, were measured in the past through intrusive techniques. The work of Netto et al. (1999), for example, used resistivity and capacitive probes. These are invasive techniques that alter the properties of a flow. An alternative technique, as shown by Van Hout et al. (2002) and Mayor et al. (2007), is the use of high speed cameras.

Van Hout et al. (2002) made a comparative study to evaluate the speed bubbles in slug flows for different slopes of the pipe, using capacitive probes and particle image velocimetry with a high speed camera. The results obtained by the two measurement techniques showed similar results, either when the bubbles travel in stagnant or moving flows. These authors calculated bubble speed using the pixel location of the nose of the bubble and the time between capturing images.

Mayor et al. (2007) also used captured images to calculate speeds, lengths of bubbles and liquid pistons in vertical pipes. In this work, different processes for the treatment of images were discussed, including gray scale conversion, filtering, subtraction, conversion to binary, erosion and the definition of the bubble shape. The work also developed expressions for the estimation of the uncertainties of some flow parameters.

The previous articles have basically determined the linear dimensions of bubbles. The present work estimates areas and volumes from two-dimensional measurements.

4. EXPERIMENTAL SET-UP

The experiments were carried out in the Laboratory of Multiphase Flows in Pipes (LEMT) of the Mechanical Engineering Program of the Federal University of Rio de Janeiro. The basic geometric arrangement consists of an acrylic pipe with 45.7 mm in diameter and 12 m in length. The pipe is placed horizontally. Other basic elements are: a water storage tank with 4 m^3, a compressor, a positive displacement pump, a frequency inverter, a Coriolis flow meter, an acrylic box filled with water, a high-speed camera DANTEC NanoSense Mk III with capacity of 2080 frames per second and resolution of 1280x1024 pixels, a source of light Motion LED synchronized to emit the light beam at the moment of capture by the camera and a rotameter. Figure 2 shows a sketch of the test facility.

ISSN 2176-5480

The water circulates in open circuit. A T-junction is used to inject the air arriving from the compressor. Phase separation is achieved in the main storage tank.

Flow patterns for 50mm-diameter pipes were used to define different combinations of water and air velocities that resulted in the desired slug flow configuration. The water flow velocity was kept constant, and by varying the valve opening of the air inlet, different results were obtained. Thus, different speeds, sizes and forms of the bubble and liquid piston lengths were achieved.

To obtain the images, an acrylic box (0.7x0.15x0.15 m, 5mm thick), was placed 8 m downstream of the entrance. The box was filled with water to reduce image distortion.

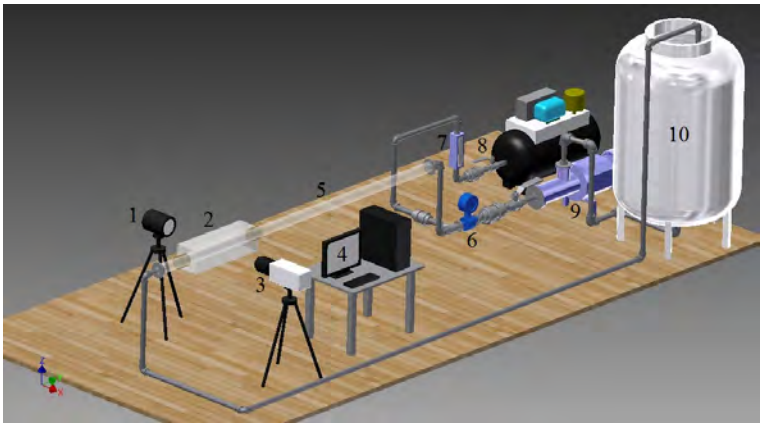

Figure 2. Sketch of the test facility.

5. IMAGE TREATMENT

To obtain the volume, dry area, wet area and interfacial area of bubbles, the computational platform WOLFRAM MATHEMATICA 8.0 was used. To set the image capture frequency, the DYNAMIC STUDIO v3.14 software was used. The steps for image processing took as basic reference the work of Mayor et al. (2007). They are here shortly reproduced for the sake of completeness and to clarify the present procedure.

5.1 Evaluation of the speed of the bubble

To evaluate the speed of bubbles, images were obtained with a capture frequency of 100 Hz. Pictures were then used to determine two successive positions (s_2, s_1) of the nose at two different instants of time (t_2, t_1). Velocity was estimated from $V = (s_2\text{-}s_1)/(t_2\text{-}1_1)$. When the flow is fully developed, the velocities of the nose and of the tail are nearly the same. Velocities were considered consistently determined when differences between nose and tail velocities did not exceed 3%. Figure 3 shows the initial and final position of the nose and tail.

5.2 Frequency of capturing images

Given the bubble velocity, the capture frequency for long bubbles was defined. The frequency of capture (f_c) was determined by dividing the velocity of the bubble by the image frame length.

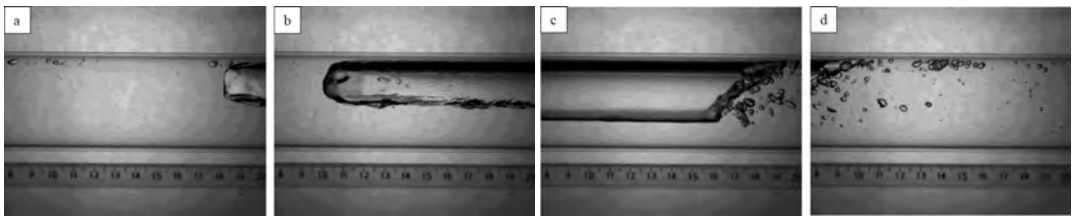

Figure 3. (a) Initial position of the nose, (b) final position of the nose, (c) inicial position of the tail, (d) final position of the tail.

Finding f_c was a critical step for bubble reconstruction. Since some of the measured bubbles were as long as $130D$, as many as 50 image frames needed to be patched to capture the entire bubble. A typical example with bubble length spanning four image frames is shown in Fig. 3.

ISSN 2176-5480

5.3 Acquisition of images

Images are imported by WOLFRAM MATHEMATICA 8.0 in jpg format. Also, it is necessary to import the image of the pipe filled with the stagnant single-phase liquid, to perform a subtraction operation and obtain the bubble shape.

5.4 Convert to grayscale

Images are converted to gray scale with 256 gray levels (Fig. 4).

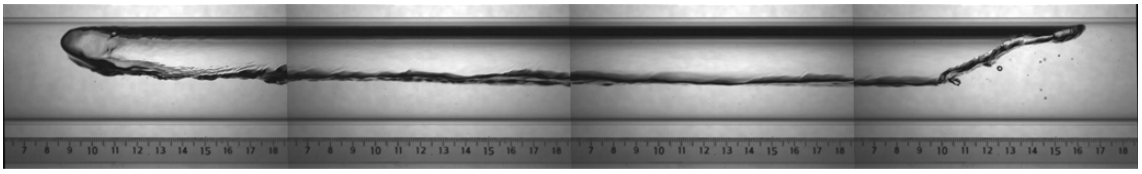

Figure 4. Bubble formed by the images.

5.5 Subtraction of images

The result of this process is an image where each pixel is obtained by subtracting the values of the corresponding pixels of the image and the image of bubble pipe with stagnant liquid. The result is detailed in Fig. 5.

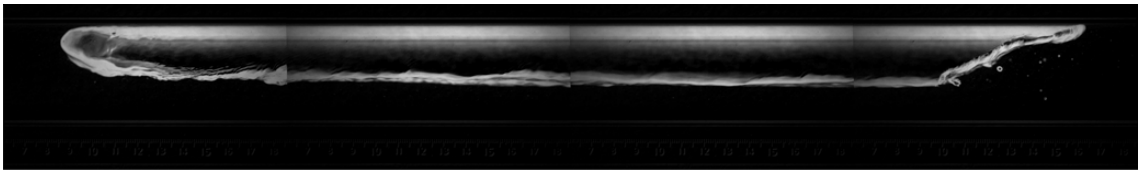

Figure 5. Subtraction process of the images.

5.6 Filter application

Implementation of the filter is necessary to remove or reduce picture noise. In this process, a median filter is applied, where each image pixel is replaced by the median of neighboring pixels.

5.7 Removal of small components

This operation eliminates small components of image usually located at the bottom of the bubble body and tail.

5.8 Conversion to a binary image

This process obtains a binary image in which the white pixels correspond to zeros and zero crossings in the image. This operation is very important to obtain the contour line, which serves for the calculation of areas and volumes of the bubble. Figure 6 shows this process.

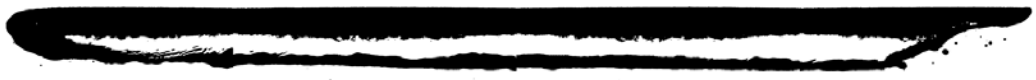

Figure 6. Binary image of the bubble.

5.9 Elimination of the inner element and of further small elements

In the last process, a white region remains inside the bubble. This region is modified through an operation that eliminates components with a given size. Figure 7 shows the result of this tool.

ISSN 2176-5480

Figure 7. Bubble shape without inner element.

5.10 Erosion image

This is a morphological image operation that changes every pixel of the image according to the values of neighboring pixels. More specifically, the erosion sets the value of each pixel of the image as the minimum value of its neighboring pixels.

5.11 Obtaining the contour line

The result of this operation is a binary image of the contour line of the bubble, which has the location of the pixels required to make calculations in obtaining volumes and areas. Figure 8 explains this process.

Figure 8. Contour line of the bubble.

5.12 Obtaining the values of the contour line

The previous binary image is an array of values, where the black pixels have a value of 0 and white pixels have the value 1. Therefore, it is possible to obtain the location of each pixel of the contour for the evaluation of the volume, dry and wetted areas, and interfacial area of the bubble. Figure 9 shows the contour points that define the bubble shape.

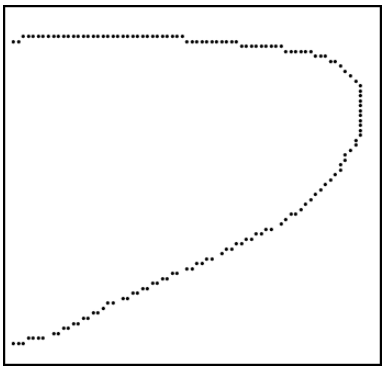

Figure 9. The contour points that define the bubble shape, detail of the tail.

5.13 Calculation of volume, dry area, wetted area interface area

With the location of pixels, cross section slices can be defined that assembled together define the three dimensional shape of the bubble. Then, simple geometric relations can be advanced to evaluate the areas and volume of individual slices. All slices added together furnish the total areas and volume of the bubble. Figure 10 depicts the scheme for the calculation of areas and volumes of the bubble.

ISSN 2176-5480

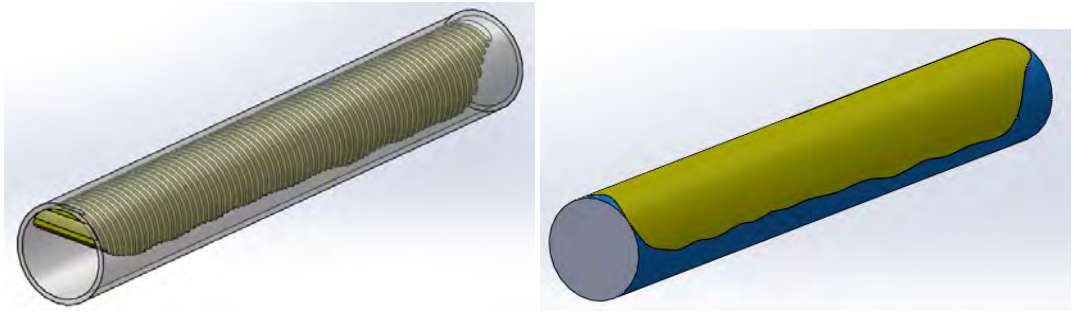

Figure 10. Areas and volumes from a series of slices.

6. LENGTH-AREA-VOLUME OF LONG BUBBLES

Interface effects can be incorporated to one-dimensional theories provided relations of the form $l = f(V^{1/3})$ and $A = g(V^{2/3})$ can be defined, where l stands for length, A for area and V for volume. The theory of Netto et al. (1999) considers regular surfaces, deprived of wrinkles or further complications. In fact, in horizontal slug flows, the gas phase always moves faster than the liquid phase. As a result, pressure and friction forces perturb the equilibrium of the flow, generating waves at the gas-liquid interface that provoke sharp fluctuations on the bubble contour and give rise to a complex pattern.

The dramatic changes on the shape of a bubble as a function of the mixture velocity are shown in Fig. 11. For small velocities ($Fr < 1$), bubbles present a short nose located at the top of the pipe and followed by perturbations on the bottom interface characterized by perturbations with a constant wavelength and decreasing amplitude (Fig. 11a-b). As Fr increases, the nose is pushed to the center position of the pipe, increases in size and shows strong perturbations on the top and bottom interfaces.

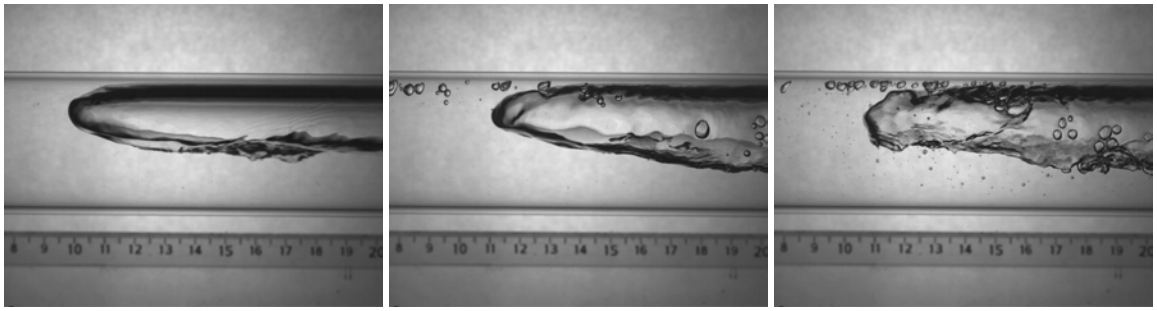

Figure 11. Typical shape of the bubble nose for various slug conditions. (a) U = 0.96 ms^{-1} (Fr = 1.43); (b) U = 1.30 ms^{-1} (Fr = 1.93); (c) U = 1.90 ms^{-1} (Fr = 2.83).

The tail structure is shown in Fig. 12. For low Fr, a mild hydraulic jump followed by a well defined tail is observed, Fig. 12a-b. For the higher Fr (Fig. 12c), a tail can no longer be noted. Instead, the hydraulic jump reaches the top of the pipe directly giving rise to the formation of a swarm of small bubbles.

Figure 13 illustrates the type of two-dimensional contour of long bubbles that is presented in literature. The intermittent line corresponds to the experimental data, whereas the smooth line corresponds to the predictions of Netto et al. (1999). Results are very good for all three bubbles. The highly intermittent interface area of the bubbles is evident.

To illustrate the three-dimensional rendering process, consider the bubble shown in Fig. 14.

A full description of the three dimensional effects on the bubble nose for high Fr is not within the scope of the present work. The complex interface perturbations seen in Figs. 11 and 12 are difficult to characterize both, experimentally and theoretically. However, a reasonable approximation can be introduced by considering the interfaces to be two-dimensional distorted surfaces. Since the working pressures are low and the difference in density between water and air is very large, gravitational effects should keep the interface at a near constant level across the transversal direction. Thus, perturbations are considered to propagate solely in the longitudinal direction.

Then, simple geometric relations can be used to construct the three-dimensional bubble presented in Fig. 15. The procedure is also used to evaluate areas and volumes.

Details of the nose and tail of the bubble shown above are depicted in Fig. 16. The distortion of the nose for the moderate Froude number is clear. The traveling perturbations shown in Fig. 16b are also clearly characterized.

A bubble subjected to a slower oncoming liquid velocity (Fr = 1.43) presents a much less perturbed nose and an

ISSN 2176-5480

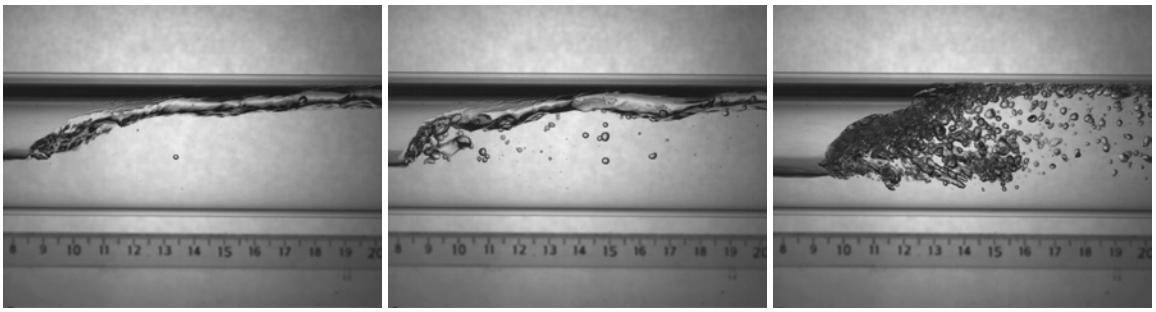

Figure 12. Typical shape of the bubble tail for various slug conditions. (a) U = 0.96 ms^{-1} (Fr = 1.43); (b) U = 1.30 ms^{-1} (Fr = 1.93); (c) U = 1.90 ms^{-1} (Fr = 2.83).

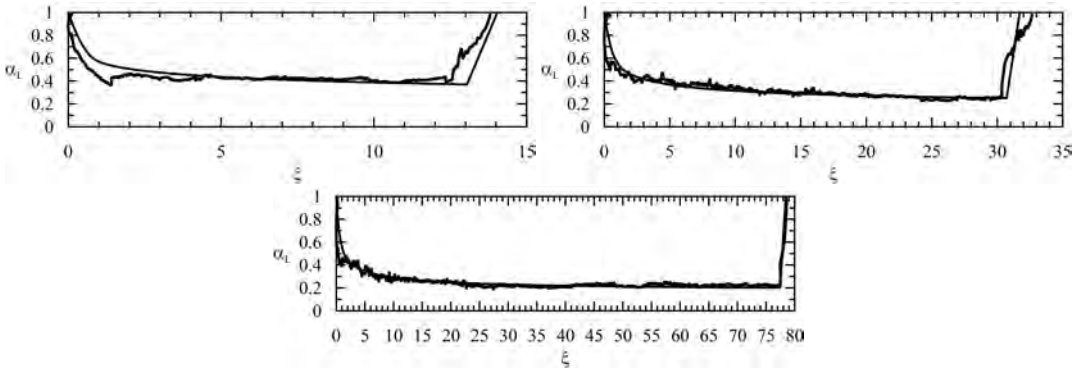

Figure 13. Typical shape of a bubble for horizontal slug flow for different bubble velocities, ξ = non-dimensional streamwise coordinate (=x/D), α_L = liquid volume fraction.

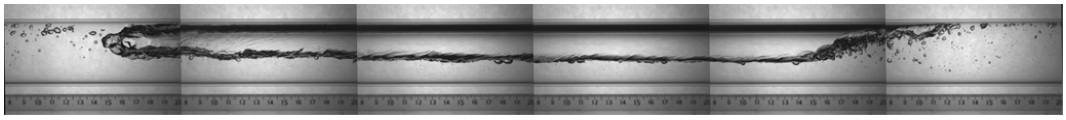

Figure 14. Two-dimensional shape of a long bubble for moderate Fr (= 1.93).

ISSN 2176-5480

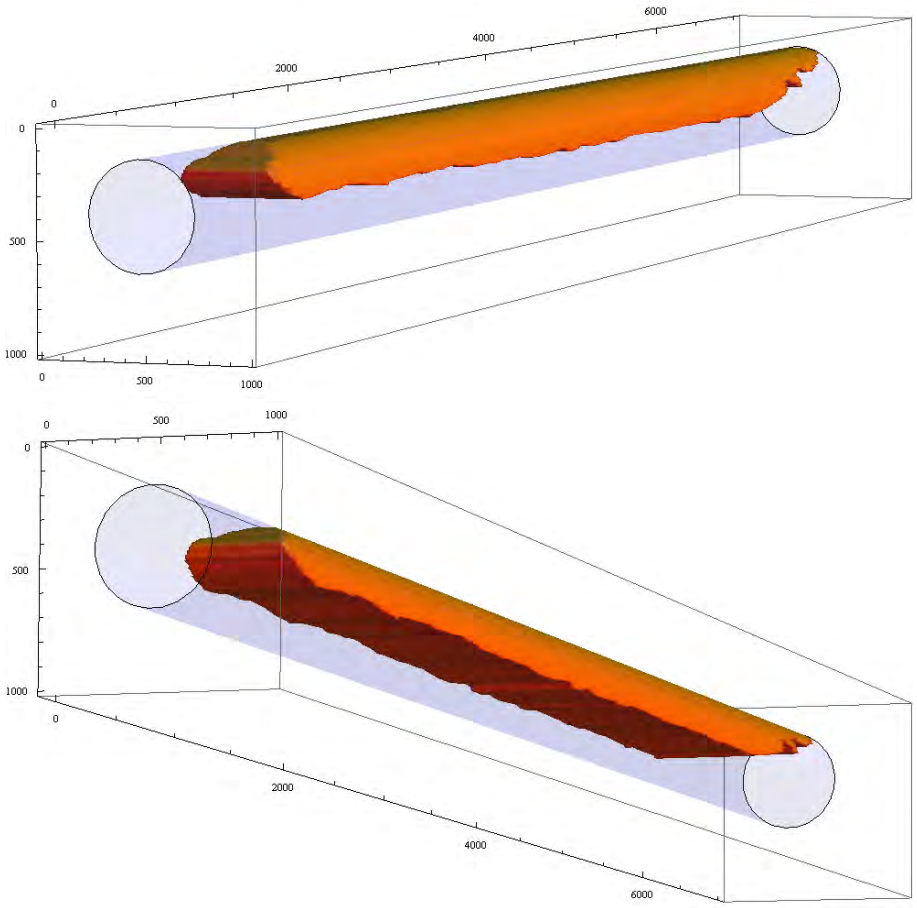

Figure 15. Three-dimensional shape of a long bubble for moderate Fr (= 1.93).

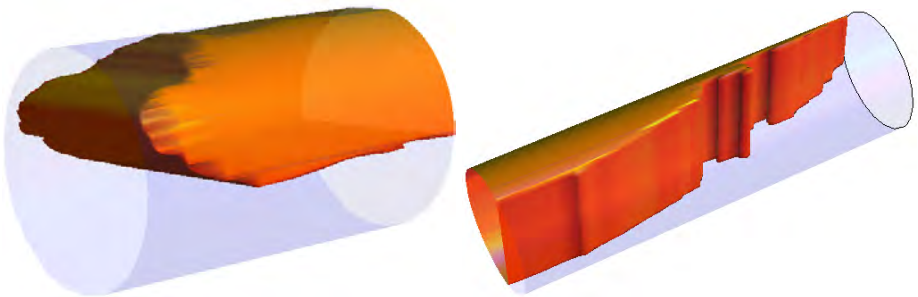

Figure 16. Detail of the nose and tail of the bubble shown in Fig. 6.

ISSN 2176-5480

elongated tail (Fig. 17).

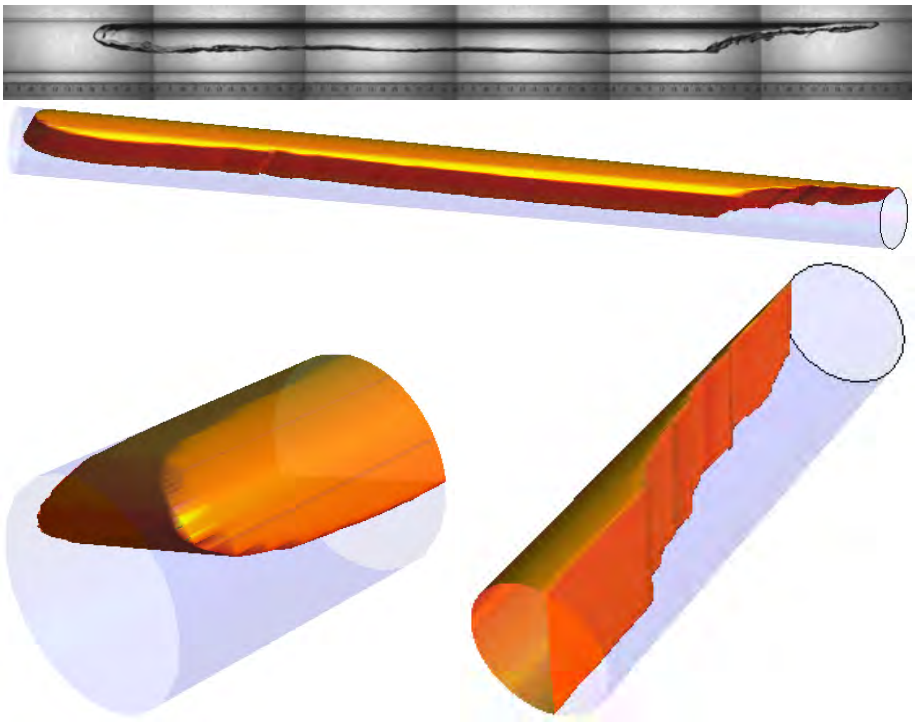

Figure 17. Three dimensional characterization of a long bubble for U = 0.96 ms^{-1} (Fr = 1.43). Details of nose and tail are also shown.

Figures 18 and 19 illustrate the relations between length-volume and interface area-volume for horizontal slug flows. Predictions furnished by the theory of Netto et al. (1999) are also shown. The agreement between experiments and theory in Figure 18 is very good. In particular, the length of long bubbles can be correlated with volumes through a power-law expression.

Because long bubbles approximate the forms of slender cylinders (limited by the cross section of the pipe), the exponent n approaches 3, indicating an almost linear relation between l_f and V.

For the interfaces, predictions are still reasonable (Fig. 19). Netto et al. (1999) show that for small Froude numbers ($Fr < 2$), the interface perturbations have a constant wavelength and a decreasing amplitude. Hence, for long bubbles the relative increase in interface area provoked by the perturbations account for a small amount, of the order of 6%. Irrespective of the range of Froude number studied in the present work, the agreement between experiments and theory for interface area prediction was not bad.

The interface area can also be reasonably described through a power-law expression, as shown in Fig. 19.

7. CONCLUSION

The present work has experimentally identified the complex structure of gas-liquid interfaces in slug flows. The work shows that the mean position of the gas-liquid interface is well characterized by the theory of Netto et al. (1999), but that complexities resulting from interface instabilities make the theoretical area predictions present about 6% below the actual values.

The areas and volumes of long bubbles in horizontal slug flows are not normally reported in literature. The present contribution has characterized bubbles with lengths varying from 4 to 130 pipe diameter. The Shadow Sizer technique has been used together with a image treatment procedure implemented in the software Mathematica^{TM}.

Two correlations are advanced to correlate lengths, interface areas and volumes in horizontal slug flows. The non-dimensional expressions have a power-law form and take as reference length the pipe diameter. Other non-dimensional lengths based on the flow dynamics were tried; however, results were not satisfactory.

8. ACKNOWLEDGEMENTS

JBRL benefited from a Research Fellowship from the Brazilian Ministry of Science and Technology through Programme Prometro (Grant No 554391/2006-6). APSF is grateful to the Brazilian National Research Council (CNPq) for the award of a Research Fellowship (Grant No 306977/2006-0). The work was financially supported by CNPq through

ISSN 2176-5480

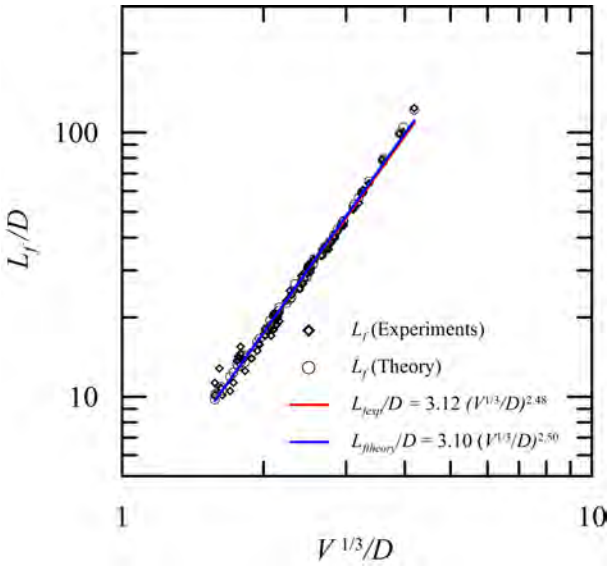

Figure 18. Length-volume relation for a horizontal slug flow.

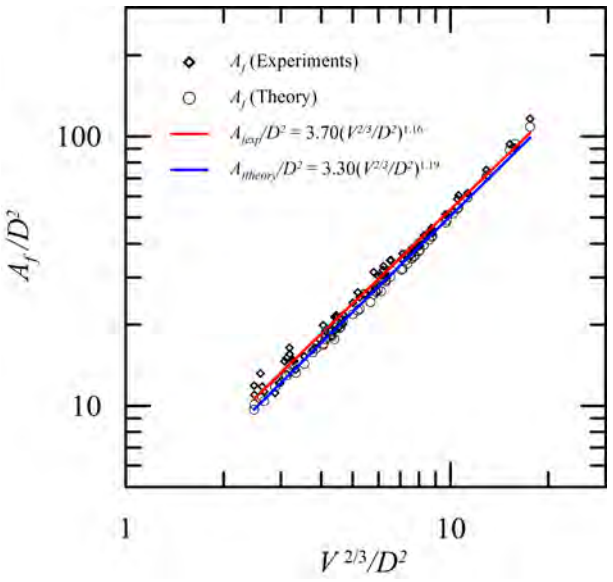

Figure 19. Gas-liquid interface area-volume relation for a horizontal slug flow.

ISSN 2176-5480

Grant No 477392/2006-7 and by the Rio de Janeiro Research Foundation (FAPERJ) through Grants E-26/171.346/2005 and E-26/171.198/2003.

9. REFERENCES

P. Andreussi, K.H. Bendiksen and O.J. Nydal, O.J., Void distribution in slug flow, *Int. J. Multiphase Flow*, vol. 19, pp. 817-828, 1993.

J.R. Fagundes Netto, J. Fabre and L. Peresson L., Shape of long bubbles in horizontal slug flow, *International Journal of Multiphase Flow*, vol. 25, pp. 1129-1160, 1999.

G.R. Magalhaes, G.F.N. Goncalves, J.B.R. Loureiro and A.P. Silva Freire, An experimental investigation of the effects of gas solubility on the properties of horizontal slug flow, *International Journal of Multiphase Flow*, vol. 50, pp. 33-40, 2013.

T.S. Mayor, A.M.F.R. Pinto and J.B.L.M. Campos, An Image analysis technique for the study of gas-liquid slug flow along vertical pipes, *Flow Measurement and Instrumentation*, vol. 18, pp. 139-147, 2007.

R. Van Hout, D. Barnes and L. Shemer, Evolution of statistical parameters of gas-liquid slug flow along vertical pipes, *International Journal of Multiphase Flow*, Vol. 27, pp. 1579-1602, 2001.

G.B. Wallis, *One Dimensional Two-Phase Flow*, McGraw-Hill, New York, 1969.